



## OPEN ACCESS

## EDITED BY

Zong Sheng Guo,  
University at Buffalo, United States

## REVIEWED BY

Gang Chen,  
University of Kentucky, United States  
Martin Frank Strand,  
Kristiania University College, Norway  
Austin Kirschner,  
Vanderbilt University Medical Center,  
United States

## \*CORRESPONDENCE

Sanjay Goel  
sanjay.goel@rutgers.edu

## †PRESENT ADDRESS

Sanjay Goel,  
Department of Medicine, Division of  
Medical Oncology, and Section of  
Solid Tumor, Rutgers Robert Wood  
Johnson Medical School, Cancer  
Institute of New Jersey, New  
Brunswick, NJ, United States

## SPECIALTY SECTION

This article was submitted to  
Gastrointestinal Cancers:  
Colorectal Cancer,  
a section of the journal  
Frontiers in Oncology

RECEIVED 13 August 2022

ACCEPTED 28 September 2022

PUBLISHED 25 October 2022

## CITATION

Augustine T, John P, Friedman T,  
Jiffry J, Guzik H, Mannan R, Gupta R,  
Delano C, Mariadason JM, Zang X,  
Maitra R and Goel S (2022)  
Potentiating effect of reovirus on  
immune checkpoint inhibition in  
microsatellite stable colorectal cancer.  
*Front. Oncol.* 12:1018767.  
doi: 10.3389/fonc.2022.1018767

## COPYRIGHT

© 2022 Augustine, John, Friedman,  
Jiffry, Guzik, Mannan, Gupta, Delano,  
Mariadason, Zang, Maitra and Goel. This  
is an open-access article distributed  
under the terms of the [Creative  
Commons Attribution License \(CC BY\)](#).  
The use, distribution or reproduction  
in other forums is permitted, provided  
the original author(s) and the  
copyright owner(s) are credited and  
that the original publication in this  
journal is cited, in accordance with  
accepted academic practice. No use,  
distribution or reproduction is  
permitted which does not comply with  
these terms.

# Potentiating effect of reovirus on immune checkpoint inhibition in microsatellite stable colorectal cancer

Titto Augustine<sup>1</sup>, Peter John<sup>2</sup>, Tyler Friedman<sup>1,3</sup>,  
Jeeshan Jiffry<sup>1</sup>, Hillary Guzik<sup>4</sup>, Rifat Mannan<sup>5</sup>, Riya Gupta<sup>1,6</sup>,  
Catherine Delano<sup>1</sup>, John M. Mariadason<sup>7</sup>, Xingxing Zang<sup>1,2,8</sup>,  
Radhashree Maitra<sup>1,9,10</sup> and Sanjay Goel<sup>1,9\*†</sup>

<sup>1</sup>Department of Medicine, Albert Einstein College of Medicine, Bronx, NY, United States, <sup>2</sup>Department of Microbiology and Immunology, Albert Einstein College of Medicine, Bronx, NY, United States, <sup>3</sup>Department of Neuroscience, Florida State University, Tallahassee, FL, United States, <sup>4</sup>Analytical Imaging Facility, Albert Einstein College of Medicine, Bronx, NY, United States, <sup>5</sup>Department of Pathology, City of Hope, Duarte, CA, United States, <sup>6</sup>Department of Computer Science, Columbia University, New York, NY, United States, <sup>7</sup>Gastrointestinal Cancers Program and Oncogenic Transcription Laboratory, Olivia Newton-John Cancer Research Institute, La Trobe University School of Cancer Medicine, Melbourne, VIC, Australia, <sup>8</sup>Department of Urology, Albert Einstein College of Medicine, Bronx, NY, United States, <sup>9</sup>Department of Medical Oncology, Montefiore Medical Center, Bronx, NY, United States, <sup>10</sup>Department of Biology, Yeshiva University, New York, NY, United States

The majority of colorectal cancers (CRCs) are microsatellite stable (MSS) and resistant to immunotherapy. The current study explores the possibility of using oncolytic reovirus to sensitize MSS CRC to immune checkpoint inhibition. While reovirus reduced metabolic activity among *KRAS*<sup>Mut</sup> cells, microarray/computational analysis revealed microsatellite status-oriented activation of immune-response pathways. Reovirus plus anti-PD-1 treatment increased cell death among MSS cells *ex vivo*. Reduced tumorigenicity and proliferative index, and increased apoptosis were evident among CT26 [MSS, *KRAS*<sup>Mut</sup>], but not in MC38 [microsatellite unstable/MSI, *KRAS*<sup>Wt</sup>] syngeneic mouse models under combinatorial treatment. PD-L1-PD-1 signaling axis were differentially altered among CT26/MC38 models. Combinatorial treatment activated the innate immune system, pattern recognition receptors, and antigen presentation markers. Furthermore, we observed the reduction of immunosuppressive macrophages and expansion of effector T cell subsets, as well as reduction in T cell exhaustion. The current investigation sheds light on the immunological mechanisms of the reovirus-anti-PD-1 combination to reduce the growth of MSS CRC.

## KEYWORDS

colorectal cancer, translational, combinatorial therapy, reovirus, anti-PD-1, immune checkpoint, microsatellite instability

## Introduction

Colorectal cancers (CRCs) with microsatellite instability (MSI) generate high levels of neoantigens due to mutations in DNA repair genes. The resulting neoantigens are detected by tumor-infiltrating lymphocytes (TILs) (1). Consequently, patients with MSI CRCs have experienced significant clinical benefits from immune checkpoint inhibition (2). Most advanced MSI cancers express high levels of immune checkpoint proteins, including PD-1, PD-L1, CTLA-4, LAG-3, and IDO, that help these cells evade immune destruction by TILs, and create an immunosuppressive tumor microenvironment (TME) (3, 4). Monoclonal antibodies targeting PD-1, otherwise called anti-PD-1, work by releasing the PD-1 receptor “brake” present on T cells. Anti-PD-1 prevents PD-1 from engaging PD-L1, a ligand expressed by tumor cells. Currently, nivolumab, pembrolizumab (anti-PD-1) and ipilimumab (anti-CTLA4) are approved by the US-FDA to treat metastatic MSI CRC (5).

MSS CRCs which typically arise due to chromosomal instability display a comparatively weaker anti-tumor immune response, resulting in these tumors being largely refractory to immunotherapy (6). As MSS CRC accounts for the majority of advanced stage CRCs (~85%) (7), sensitization of these tumors to immune checkpoint inhibition will represent a tremendous improvement in the therapeutic options available to these patients. Recent studies have identified a role for viral therapies as a promising, alternative strategy for cancer treatment. Respiratory enteric orphan virus (reovirus) is a double stranded RNA (dsRNA) virus consisting of a multilayered capsid protein structure. Our group and others have shown that reovirus preferentially replicates in *KRAS* mutant (*KRAS*<sup>Mut</sup>) cells (8), which account for approximately 45% of all CRCs (9). Reovirus enters *KRAS*<sup>Mut</sup> cells through phagocytosis, un-coats capsid proteins in endosomes where it exploits the lower levels of eukaryotic translation initiation factor 2- $\alpha$  phosphorylation in these cells to enable viral dsRNA translation. This results in increased virion assembly, progeny generation and subsequent induction of apoptosis in infected cells (10).

In addition to directly promoting oncolysis, oncolytic viruses (Ovs) can also increase the recruitment of immune cells to an otherwise immunosuppressed TME to enhance antitumor effects. The antitumor immunity influenced by antiviral response is less clear across viral platforms and tumor types (11). After the entry and replication within tumor cells, the virus eventually lyses the cells and releases tumor antigens into the blood stream. These antigens can be detected by the immune system and draw T cells into the TME to initiate cancer cell killing, and potentially trigger the system to recognize metastatic disease elsewhere in the body (12). This opens an avenue to combine reovirus treatment with ICIs in order to potentiate the efficacy of immunotherapy. Efficacy of both ICIs and Ovs

depends on factors such as cancer subtype, PD-1/PD-L1 expression, and the immune milieu (13).

In metastatic CRC (mCRC), reovirus is currently in clinical development to treat *KRAS*<sup>Mut</sup> as monotherapy or in combination with chemotherapy, however its potential to enhance the efficacy of immune checkpoint inhibitors has not been previously investigated (8). In this study, we tested the hypothesis that reovirus infection would lead to innate and adaptive immune responses and sensitize MSS CRC to PD-1 therapy, by administering reovirus as a single agent or in combination with an anti-PD-1 monoclonal antibodies in various *KRAS* wild type (*KRAS*<sup>WT</sup>) and mutant (*KRAS*<sup>Mut</sup>) CRC cell lines, and in syngeneic mouse models of CRC (14). All cell lines were separated based on *KRAS* and mismatch repair (MMR) status (Supplementary Table 1) (15, 16). We observed significantly reduced tumor progression and increased survival of animals treated with the combination regimen and elucidate the mechanistic basis for this effect.

## Materials and methods

### Cell culture and reagents

Fifty-nine human- and two mouse-origin CRC cell lines were obtained from a range of sources (15–17). Human cell lines were cultured in MEM, CT26 in RPMI 1640, and MC38 in DMEM, all supplemented with 10% FBS, 10 mM L-glutamine, and penicillin (100  $\mu$ g/mL)–streptomycin (0.1 mg/mL), at 37 °C under 5% CO<sub>2</sub> pressure. Cell line authentication was performed using GenePrint<sup>®</sup> 10 System and Fragment Analysis, and StemElite ID System (Promega, USA) at the Queensland Institute of Medical Research DNA Sequencing and Fragment Analysis Facility, Australia (January 2013) and the Genomic Core Facility, Albert Einstein College of Medicine, New York (June 2018).

### Reovirus infection

Reovirus type 3 dearing strain (Reolysin<sup>®</sup>) was provided by Oncolytics Biotech Inc. (Calgary, Canada). Based on our previous studies, 0.5 to 2  $\times$  10<sup>6</sup> cells (depending on the assay) were treated with reovirus multiplicity of infection (MOI) of 5. Cells were washed with PBS and harvested after 12 and 24 hours for downstream analyses (16, 17).

### Syngeneic *in vivo* models and allografts

Male and female BALB/c and C57BL/6 mice 6–8 week of age were purchased from Envigo Research Models & Services, NA

Inc. All animal care and experimental procedures were performed in accordance with protocols approved by the Albert Einstein College of Medicine's Institutional Animal Care and Use Committee (IACUC). BALB/c and C57BL/6 mice were intradermally injected with  $5 \times 10^5$  CT26 and MC38 cells/mouse, respectively, suspended in 100  $\mu$ L PBS on the flank region. After the tumors had reached approximately 100 mm<sup>3</sup> in size, mice were divided into four groups (n = 8-10 per group) and treated with either reovirus intratumorally (i.t.) at a daily dose on 10 million tissue culture infective dose<sub>50</sub> (TCID<sub>50</sub>) in 100  $\mu$ L PBS [Reovirus group]; anti-mouse PD-1 (CD279) antibody (Clone: RMP1-14) intraperitoneally (i.p.) twice a week 200  $\mu$ g in 100  $\mu$ L PBS [anti-PD-1 group]; reovirus plus anti-PDI [Combination group]; or 100  $\mu$ L PBS daily i.t. and isotype rat IgG2a  $\kappa$  200  $\mu$ g in 100  $\mu$ L of PBS twice a week i.p. [Control group]. We derived doses and durations based on previous studies (16, 18). Tumor volume was measured every three days using calipers and calculated as follows: volume = longest tumor diameter  $\times$  (shortest tumor diameter)<sup>2</sup> / 2 (14). Animals were euthanized and tumors were excised upon reaching a tumor volume of 2 cm<sup>3</sup> size. For survival analyses, the health and behavior of the mice were assessed daily for the duration of the study. Upon presentation of defined criteria associated with tumor burden and disease progression (abnormal feeding behavior, diminished response to stimuli and failure to thrive), mice were humanely euthanized according to approved IACUC guidelines and survival time was recorded. At the end of respective experiments, cultured cells and tumors were resected and either snap frozen or fixed in 10% buffered formalin for subsequent analyses.

## Cell viability assay

To determine reovirus sensitivity, 5,000-10,000 cells/well were seeded in 96-well plates. After 12-14 hrs, cells were treated with reovirus at a 5 MOI for 24 hrs. For each cell line, one plate was harvested at the time of viral infection for determination of t = 0 absorbance values. Viable cells were determined post treatment using the 3-(4,5-dimethylthiazol-2-yl)-2,5-diphenyltetrazolium bromide (MTT) (Sigma-Aldrich, USA; Cat# M2128) assay by measurement of absorbance at 570 nm (17). The relative rate of cell growth for each cell line was factored into the analysis by subtracting the absorbance at time 0 from both the control and treatment groups. All experiments were repeated at least three times, and each experiment was performed in technical triplicate.

## Flow cytometry

To detect the expression of surface receptors and intracellular markers, cells were washed and incubated on ice

for 20-40 minutes with appropriate fluorochrome-conjugated antibodies or isotype controls (Supplementary Table 2). Flow cytometric analysis was performed on a BD LSR II cell analyzer (BD Biosciences, USA), and the data analyzed using FlowJo version 9.1 (Tree Star, USA). For flow cytometric cell sorting, cells were stained with specific antibodies and separated on a BD FACSAria cell sorter (BD Biosciences, USA) (18, 19).

## RT-qPCR

Total RNA was isolated from cell lines and tumor tissues using the RNeasy kit (Qiagen, USA) according to the manufacturer's protocol. First-strand cDNA was synthesized using the iScript kit (Bio-Rad, USA). 10 ng of synthesized cDNA was used as template in real-time qPCR reactions using PowerUp SYBR Green (ThermoFisher, USA) on a Bio-Rad CFX96 RT-PCR machine. Changes in target gene expression were calculated using the 2- $\Delta\Delta$ CT data analysis method by comparing to the level of expression of GAPDH. Primer sequences are provided in Supplementary Table 2.

## Transcriptome profiling using microarrays and computational analysis

Eighty nanograms of excellent quality RNA (RNA integrity number of  $\geq 7.9$ ) was hybridized on Clariom S gene expression arrays that interrogate the expression of > 20,000 transcripts. The study was carried out at the Genomic Core Facility, Albert Einstein College of Medicine. The arrays were scanned using a high-resolution GeneArray Scanner 3000 7G (ThermoFisher Scientific, USA). Data processing, normalization, background correction and array quality control were performed using Affymetrix's Transcriptome Analysis Console (TAC). Annotation of probes was performed using the clariomshumantranscriptcluster.db package, and the average expression level was calculated for probes, which mapped to the same gene. For comparisons between groups, *Limma* package was used to perform an eBayes-moderated paired t-test provided in order to obtain log<sub>2</sub> fold change (log<sub>2</sub>FC), p value, and adjusted p value (Benjamini-Hochberg-calculated FDR) (20). Genes that displayed statistically significant tests (p value < 0.05 and fold change [FC]  $\geq 1.5/\leq -1.5$ ) were considered differentially expressed (DEGs). Deconvolution analysis was performed using 847 immune-response related genes identified earlier by our group (21, 22).

Gene ontology (GO) terms and KEGG pathway enrichment analysis of DEGs: Analysis of GO terms such as biological process, cellular component, and molecular function were performed using the online tool DAVID (<https://david.ncicrf.gov>) to identify systematic and comprehensive biological/cellular functions and conduct pathway exploration. The Functional Annotation setting in DAVID, which includes GO enrichment and use of the Kyoto

Encyclopedia of Genes and Genomes (KEGG) pathways, helps to identify enriched genes among the list and uses previously annotated genes from the Clariom S array as background. GO categories with p value of < 0.05 and FC  $\geq 2/\leq -2$  were considered to be significantly enriched (23).

Protein–protein interaction (PPI) network analysis: To identify the hub regulatory genes and to examine the interactions between the DEGs, a PPI was generated using STRING (<https://string-db.org/>). These genes required an interaction score  $\geq 0.2$  and a maximum number of interactors = 0. The genes and corresponding PPI were imported into Cytoscape (version 3.6.1) with the Molecular Complex Detection (MCODE) app (version 1.5.1) to screen and visualize the modules of hub genes with a degree cut-off = 2, haircut on, node score cut-off = 0.2, k-core = 2, and max. depth = 100 (23).

## Transcriptome profiling using RNA-seq

RNA-Seq analysis of 59 CRC cell lines was performed at the Australian Genome Research Facility (Melbourne, Australia) on an Illumina HiSeq2000 to a depth of >100 million paired reads as previously described by Mouradov et al., 2014 (24). Absence of gene expression was defined as a RPKM value of <1 (25, 26).

## Western blotting

Total cellular proteins were extracted using RIPA buffer and by solubilizing the proteins by boiling in SDS buffer (50 mM Tris-HCl, pH 7.5, 150 mM NaCl and 1% SDS). Protein lysates were then separated on an 8%–12% SDS-polyacrylamide gel. The proteins were then transferred to PVDF membrane (Millipore, USA) and incubated overnight at 4 °C with antibodies (Supplementary Table 2). Signal detection was performed using enhanced chemiluminescence (GE Healthcare, USA) (17).

## Ex vivo co-culture and real-time quantitative live-cell imaging

The IncuCyte S3 Live-Cell Imaging system (Essen Bioscience, USA (27)) was used for kinetic monitoring of cytotoxicity and apoptotic activity of CRC cell lines. CRC cells were seeded at a concentration of 4000 cells/well in a 96-well ImageLock™ plate (Essen BioScience), incubated overnight, and co-cultured with healthy human PBMCs at a ratio of 1:5 for 24 hrs. Cells were transfected with NuLight Green BacMam 3.0 Reagent and Cytotox Red Reagent (dead cell counting). After 24 hrs, cells were treated with PBS, reovirus (2 MOI), anti-human

PD-1 mAb (nivolumab; 2 nM) (16, 28), or a combination of reovirus and anti-human PD-1 (Supplementary Table 3). Plates were scanned and fluorescent and phase-contrast images were acquired in real-time in every 2 hrs from 0 to 144 hrs post treatment. Normalized green object count per well at each time-point and quantified time-lapse curves were generated by IncuCyte S3 2017A software (Essen BioScience). Cytotoxicity was calculated as Cytotox Red-positive cells divided by total cells per field, then divided by t = 0 (29). The assays were performed on green-red overlay to quantify the number of cells that were dying through interactions of reovirus, anti-human PD-1, and their combination.

## Tumor microarray (TMA), immunohistochemistry (IHC) and immunofluorescence (IF)

Mouse tissue procurement: At the end of *in vivo* experiments, aliquots of tumor tissues were formalin fixed and paraffin embedded. Slides of tumor samples stained with hematoxylin and eosin were independently reviewed by a pathologist, and representative areas were marked. Core tissue biopsy specimens (2 mm in diameter) were obtained in triplicates from individual paraffin-embedded samples (donor blocks) and arranged in a new recipient paraffin block (tissue array block) using a tissue microarray construction punch needle (Newcomer Supply, USA). Each tissue array block contained up to 60 specimens, which allowed all 120 specimens (triplicate specimens of 20 cases) to be contained in 2 array blocks. Sections (4- $\mu$ m) were cut from each tissue array block, placed on slides and deparaffinized, and dehydrated. IHC was performed as previously described (30). In brief, antigen retrieval was performed by microwaving 4- $\mu$ m sections in 0.01 M citrate buffer, pH 6.0, for 15 min at 650 W. Endogenous peroxidase activity was quenched with 3% hydrogen peroxide in methanol for 15 min. After incubating sections with blocking solution for 10 min, primary antibodies (Supplementary Table 2) were added at 4°C for 12 h followed by biotinylated secondary antibody at room temperature for 10 min, and then streptavidin horseradish peroxidase (HRP) for 10 min. Staining was carried out with diaminobenzidine (DAB) chromogen, and counter-staining with Mayer's hematoxylin. Blocking solution, secondary antibody, streptavidin HRP, and DAB were all purchased from the Cap-Plus Kit (Zymed Laboratories, USA). Stromal cells surrounding the tumor area served as internal positive controls.

Immunofluorescence was carried out using methods previously described (31). DAPI counterstain to identify nuclei and Cy-5-tyramide detection for target (C35, 1:500 dilution; Vaccinex, USA) for compartmentalized analysis of tissue sections were performed. Images of each TMA core were

captured using a confocal microscope (Leica Microsystems, USA), and high-resolution digital images analyzed by the CaseViewer v.2.3 software (3D Histech, Hungary). While the number of tissues analyzed varied between different groups and species, all samples were in triplicate and  $n=7$  per group as an average. We procured 2 sets of blocks per condition. Tumor staining was scored by a trained pathologist who had no knowledge about the data. The sections were scored semi quantitatively by light microscopy, using a 4-tier scoring system: 0, no staining; 1, weak staining; 2, moderate staining; 3, strong staining. In addition, the percentage of staining was also scored: 1 (0-25%); 2 (26-50%), 3 (51-75%) and 4 (76-100%). The final score for each section was obtained by multiplying the 2 scores.

## Statistical analysis

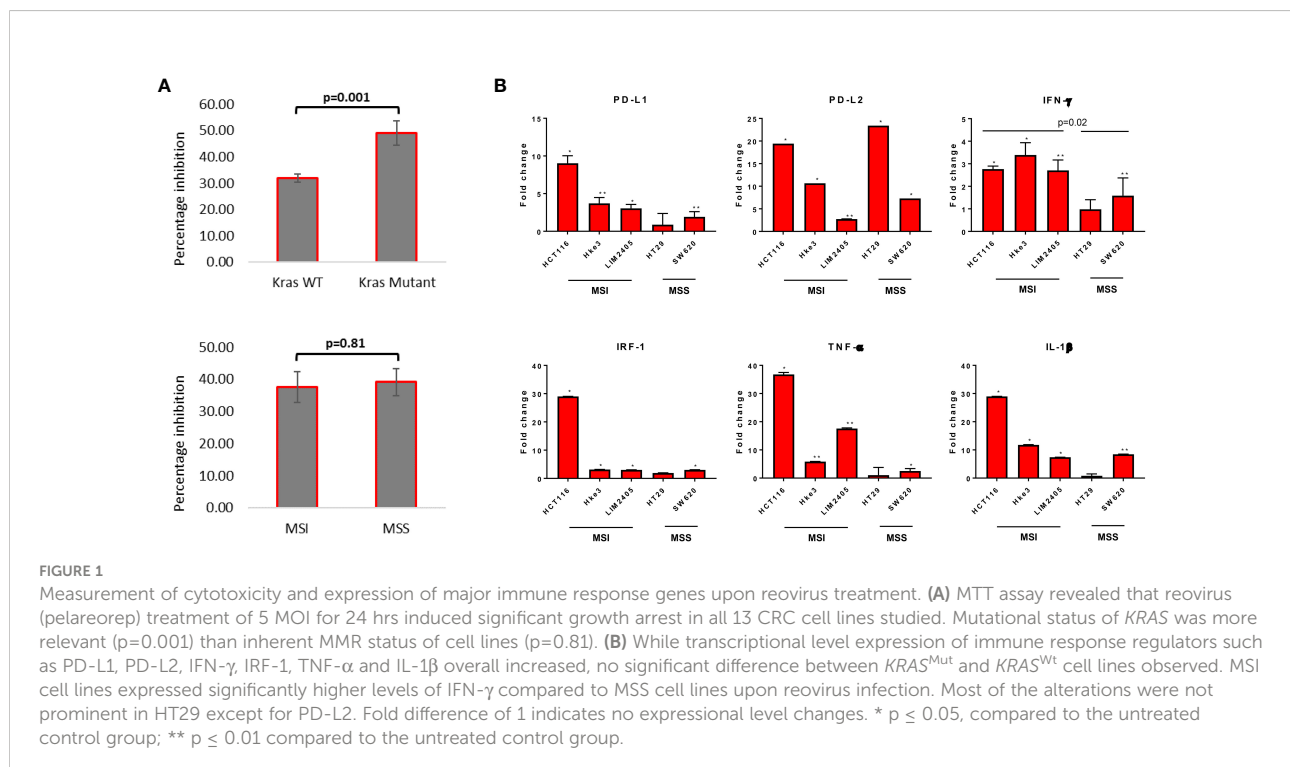
All data are presented as mean  $\pm$  SEM of the indicated number of experiments. Differences were analyzed by Student's *t*-test or ANOVA and Fisher's *post-hoc* multiple comparisons test in Microsoft Excel or GraphPad Prism programs. Survival data was analyzed with the Kaplan–Meier and log-rank tests for survival distribution. Results were considered significant when  $p \leq 0.05$ .

## Results

### Reovirus infection reduces cell viability and activates key immune-response genes among cell lines

To assess differential sensitivity to reovirus, thirteen CRC cell lines were treated, and cell viability was assessed by MTT assay. The Caco-2 cell line ( $KRAS^{Wt}$ , MSS) was found to be the most refractory to reovirus infection (75.5% cell survival after 24h) and HCT116 cells ( $KRAS^{Mut}$ , MSI) the most sensitive (29.3% cell survival). Reovirus preferentially induced growth inhibition in  $KRAS^{Mut}$  cell lines ( $p=0.001$ ), while no difference in sensitivity was observed between MSS and MSI lines (Figure 1A and Supplementary Figure 1).

We next assessed the effect of reovirus treatment on expression of immune-response related genes by RT-qPCR analysis. Significantly increased expression of immune response related genes, including PD-L1 and PD-L2, and also IFN- $\gamma$ , IRF-1, TNF- $\alpha$  and IL-1 $\beta$ , in presence of reovirus was observed (Figure 1B). HCT116 had  $\geq 20$ -fold increase in the transcription of PD-L2, IRF-1, TNF- $\alpha$  and IL-1 $\beta$ . Overall, 5 MOI reovirus treatment for 24 hours prompted significant growth reduction and expression of key immune-response genes among CRC cell lines.



## Microarray followed by bioinformatic analysis reveal inherent differences in primary immune responses between MSI/MSS tumors upon reovirus administration

To investigate the transcriptional reprogramming induced by reovirus infection, four CRC cell lines - HCT116, Hke3, SW620 and Caco-2 were infected with reovirus, and gene expression changes were assessed by microarray analysis 24 hours post-reovirus infection (Figure 2 and Supplementary Figure 2). Hierarchical-clustering of reovirus-induced changes in expression of global immune genes were identified. The differentially expressed genes (DEGs), and the correlated pathways of virus mediated immune responses were determined. We observed an increased number of DEGs under MSI/MSS classification when compared to  $KRAS^{Mut}/KRAS^{Wt}$  (Figure 2A and Supplementary Figure 2A).

Next, the Gene ontology (GO) terms and KEGG pathway enrichment analysis of DEGs revealed that tumor necrosis factor (TNF), NOD-like receptor (NLR), NF- $\kappa$ B signaling, and viral carcinogenesis pathways are associated with MMR status, while

immune system processes are primarily associated with  $KRAS$  classification (Figure 2B and Supplementary Figure 2B). Using string database, we further analyzed the Protein-protein interaction (PPI) network to identify the hub regulatory genes and to examine the interactions between the DEGs in MSI, MSS,  $KRAS^{Mut}$  and  $KRAS^{Wt}$  using the MCODE plugin in Cytoscape. These findings displayed the prominently upregulated genes that were involved in our samples. To explore the functions of these genes, we further investigated for proteins that interact with the DEGs in STRING and constructed subsequent PPI networks (Figure 2C and Supplementary Figure 2C).

The hub gene networks, also illustrated that cAMP responsive element binding protein 1 (CREB1) gene was highly upregulated under reovirus treatment in any circumstance or independent of genotypical characteristics (Figure 2D and Supplementary Figure 2D). Reovirus infection prominently activates programmed cell death among MSI, and innate immune response pathways among MSS cells, which were important regulators of NLR signaling (32), a function completely absent from the results of  $KRAS^{Mut}$  vs  $KRAS^{Wt}$  comparison using DAVID and STRING database analysis. In

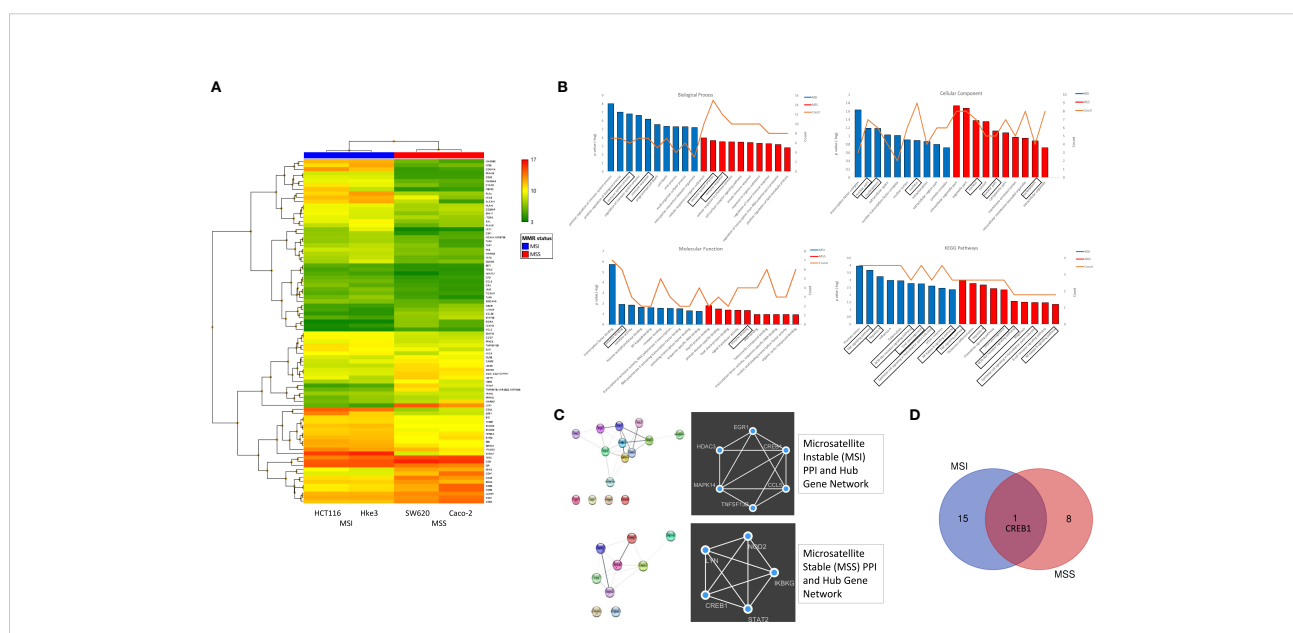


**FIGURE 2**

Differential expression of global immune response genes under reovirus infection in CRC cell lines categorized on MMR status. **(A)** Hierarchical-clustering profile across differentially expressed genes (DEGs) participating in immune pathways upon treatment with reovirus in MSI and MSS groups. RMA normalized expression values for the 86 genes were used to generate a heat-map in the TAC software. The colors indicate the expression value relative to the median expression value per gene in the dataset. Red indicates upregulation relative to median value and green indicates downregulation relative to the median value. **(B)** GO term enrichment and KEGG pathway analyses of DEGs using DAVID. Differentially expressed probes between MSI and MSS cell lines treated with reovirus were selected based on meeting the criteria of  $p \leq 0.05$  and divided into positive and negative fold changes lists and used to determine enrichment. **(C)** Protein interaction analysis using STRING. The different colored nodes represent different genes. Different edges (lines) show the interplay between genes. Edge strength is shown by thickness of the line, the thicker the line, the stronger the interaction. Hub networks made using MCODE demonstrate the genes within the PPI that were screened to display the most highly upregulated. The genes not included in the hub networks did not have substantial interaction amongst the other genes in the list, therefore they were not included. **(D)** Venn diagram created using the TAC software. It illustrates the clear point that between the MMR subgroups, CREB1 gene is the only commonality out of 25 genes, 16 in the MSI and 9 genes in the MSS groups.

summary, specifically enriched GO terms such as positive regulation of immune system function, regulation of innate immune response, and innate immune response serve as indicators of involvement of T cell regulation (33) under MSI/MSS classification. This paved the way to hypothesize that immune-related genes are highly expressed under reovirus treatment in our samples and can be taken towards the advantage of successful application of ICI as a partner drug to treat MSS type CRC.

### Combinatorial administration of reovirus and anti-human PD-1 mAb increases cell death among MSS lines in *ex vivo* co-culture models

With the above information, we sought to determine whether reovirus treatment can enhance the anti-tumor

efficacy of anti-PD-1 in co-cultures of cancer cells and PBMCs. In order to do this, we first studied stemness markers in the above-mentioned cell lines, as these are associated with increased aggressiveness, tumor mass formation, and metastasis in CRC. We analyzed putative surface proteins CD133, CD44, CD24, and CD326/EpCAM (epithelial intracellular adhesion molecule) (34) and connected the findings with their sensitivity to reovirus. Using RNA-Seq analysis, we studied the expression of stemness markers in 59 human CRC cell lines (Figure 3 and Supplementary Figure 3). All 4 genes analyzed had well-defined expression in cell lines [RPKM >1 in at least 3/13 CRC cell lines by RNA-Seq] (total of n=20,702 genes). Nine cell lines that had abundant expression of stemness markers were chosen and validated using flow cytometry analysis (Figure 3A). The cell lines LIM2405, HCT116, Caco2, HT29, SW620 and SW837 had increased expression of stem cell markers, with Caco2 that had low CD24 expression being an exception and were selected for further studies. KM12, LIM1215 and RKO had overall reduced

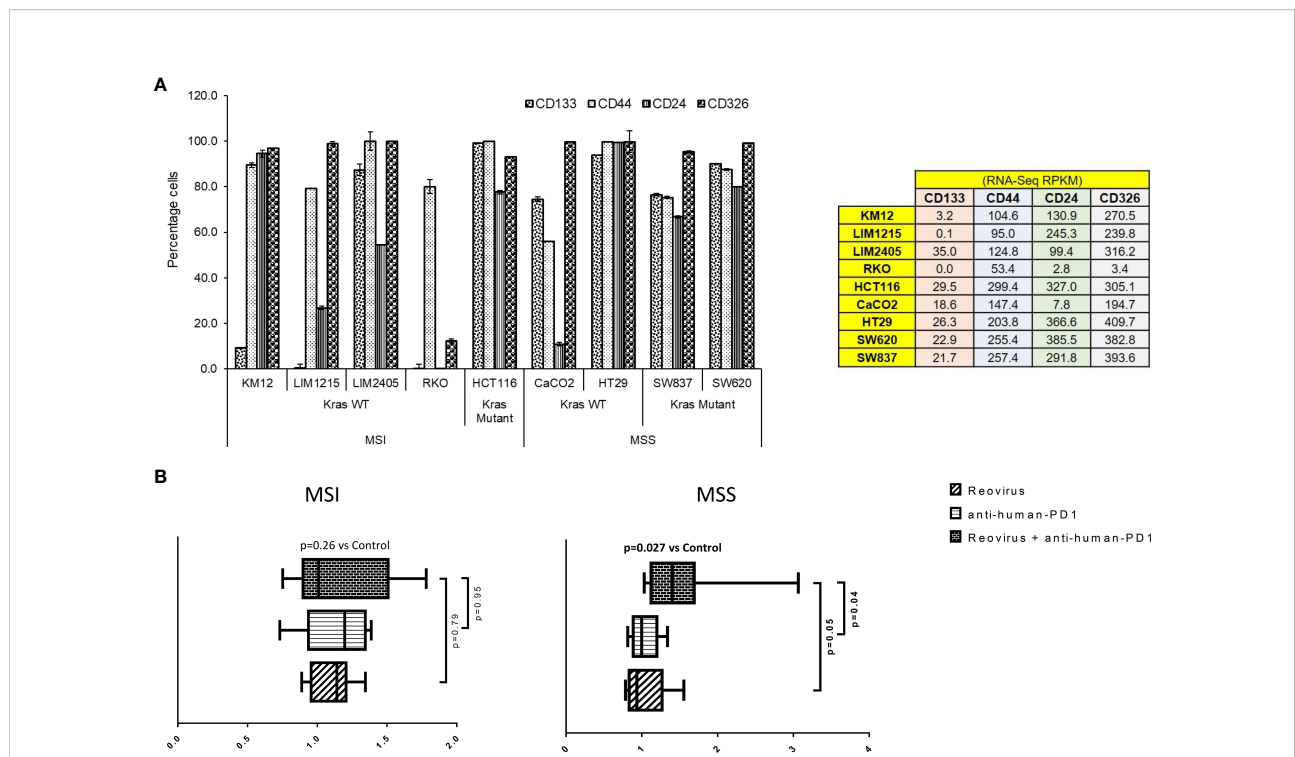


FIGURE 3

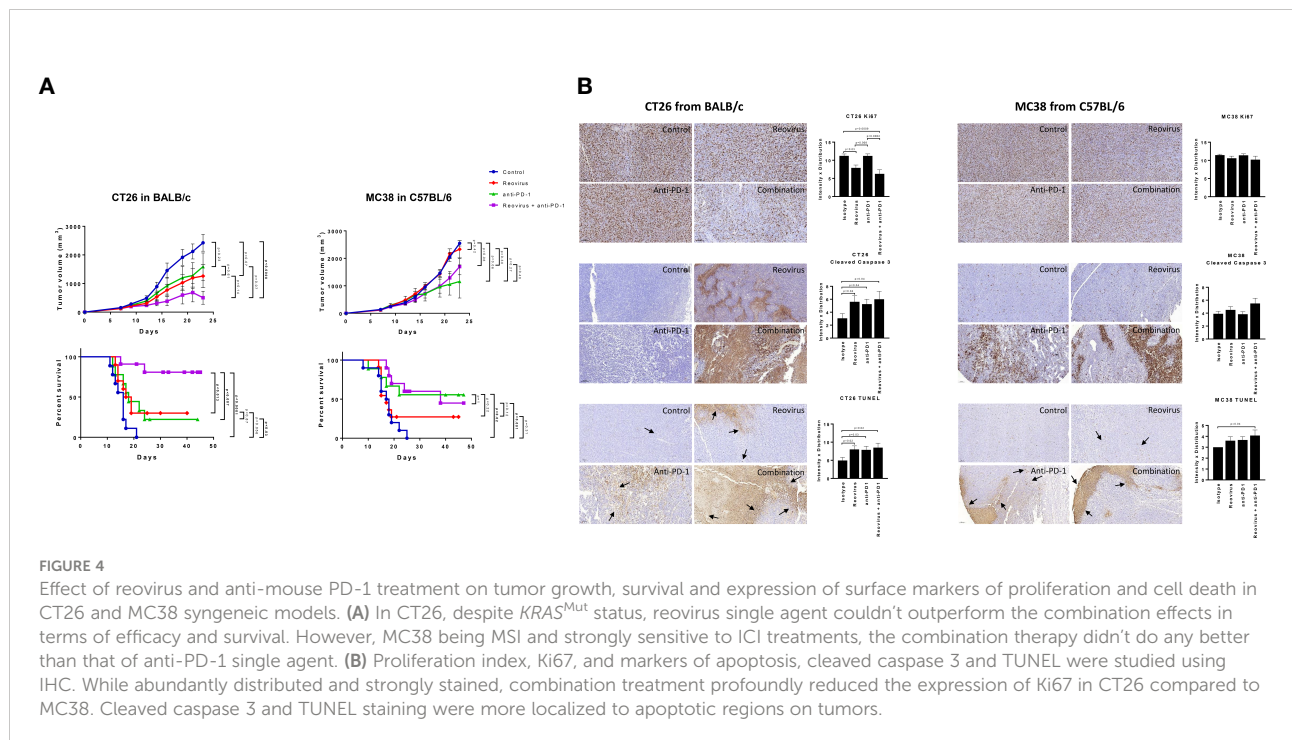
Selection of CRC cell lines, measurement of cytotoxicity, live-cell imaging and analysis in an *ex vivo* co-culture system. (A) Human CRC cell lines were selected based on expression of epithelial and stemness markers, and sensitivity towards reovirus infection. Out of 59 CRC cell lines screened using RNA-Seq (Supplementary Figure 2), nine highly expressing ones (values are indicated on right panel table) with increased sensitivity to reovirus (Figure 1A and Supplementary Figure 1) were chosen and subjected to confirmatory analyses. One cell line per condition based on statuses of MMR and KRAS mutation with top expression of epithelial and stemness markers was taken for *ex vivo* co-culture studies (n=8). (B) Levels of cell death among MSI and MSS CRC cell lines co-cultured with human PBMC (1:5) and treated with reovirus, anti-human PD-1 and their combination. Trends in fold difference and significance are depicted on box and whisker plot. Combination treatment compared to placebo rendered significant improvement in cell death only in MSS group. Combo increased cell death 1.6-fold in MSS and 1.2-fold in MSI (p values in bold letters indicate significance). Single agent treatments resulted in more than 1-fold cell death in all groups. Details of cell death was captured using live-cell imaging system and provided under *Supplementary Movie* section.

expressions of markers. In general, MSS had noticeably high expression of these markers compared to MSI.

We next performed *ex vivo* co-culture (1:5 CRC cells to healthy PBMC ratio) experiments using reovirus and anti-human PD-1 mAb and quantitatively determined cell death by 2 hourly live-imaging for 144 hrs. MSS cells (SW620 and HT29) underwent significant cell killing in response to combinatorial therapy (2 nM nivolumab plus 2 MOI reovirus) when compared to control/placebo treatment (Figure 3B). While single agent reovirus failed to show any significance compared to placebo or combination treatment, the difference between anti-human PD-1 administration and combination was significant. No significant difference was observed between anti-human PD-1 and placebo treatment among MSS cell lines. Further, only MSS cell lines collectively showed significantly increased cell death upon combination treatment (Figure 3B and Supplementary Figure 4). We performed phase-contrast live-cell imaging (Cytotox Red uptake) over a 144-hr period to characterize the kinetics of the cytotoxicity of reovirus and anti-human PD-1 towards CRC cell lines, HT29, SW620, LIM2405 and HCT116. The study demonstrated that combination-treated cells exhibit distinct cell morphology compared to untreated cells. Reovirus-treated cells showed membrane ballooning followed by membrane rupture while combination-treated cells displayed classical features of apoptosis such as cell shrinkage and membrane blebbing (apoptotic body formation). This unique morphology suggests combination-induced cell death is not distinct from apoptosis and is specific to MSS (HT29) cells (Supplementary Movie).

### Differential effectiveness of reovirus and anti-PD-1 treatment in CT26 and MC38 syngeneic models of CRC

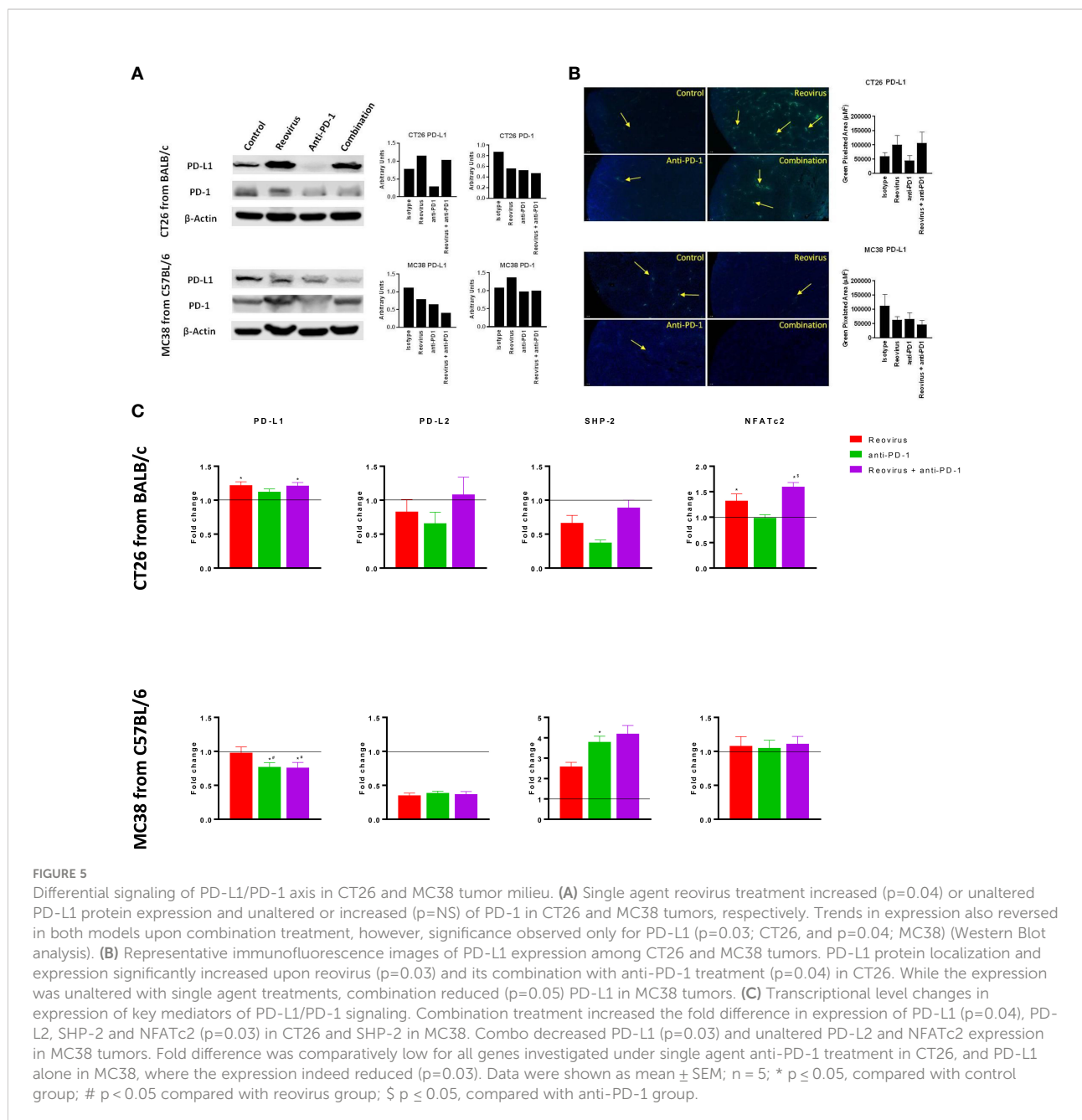
The effect of combining reovirus with an anti-PD-1 mAb on colon tumor growth was next examined *in vivo* using the CT26 (in BALB/c) and MC38 (in C57BL/6) syngeneic mouse models. In the *KRAS*<sup>Mut</sup> CT26 model, single agent reovirus or anti-PD-1 treatment induced a modest decrease in tumor growth, however these effects were not statistically significant. Comparatively, combined treatment with reovirus and anti-PD-1 induced a highly significant suppression of the growth of established CT26 tumors. Consistent with the attenuation of tumor growth, combined reovirus/anti-PDL1 treatment significantly prolonged survival of mice harboring CT26 tumors. Comparatively, no significant differences in tumor growth or survival were observed in *KRAS*<sup>Wt</sup> and MSI MC38 model, where single agent anti-PD-1 treatment showed significantly improved therapeutic response compared to controls. Reovirus treatment alone had modest response in terms of altering survival rate or tumor sizes. Combined treatment, while was nonresponsive up to ~16 days, showed poorer capability to reduce tumor sizes compared anti-PD-1 single agent treatment. To assess the toxicity induced by reovirus and anti-PD-1, body weight was monitored throughout the treatment period and necropsy was performed on one mouse from each group at the conclusion of the study (after 22 days of treatment; endpoint) (Figure 4A).



## Combinatorial treatment reduces the proliferative index and increases programmed cell death in CT26 tumors

To understand the mechanism driving the anti-tumor activity of the reovirus/anti-PDL1 treatment, resected tumors were stained for the proliferation marker, Ki67, and apoptosis markers cleaved-caspase 3 and TUNEL (Figure 4B representative images). Nuclear expression of Ki67 was decreased in reovirus and combination treated groups compared to isotype-treated controls in both models. However, the differences were significant only in CT26

model. Anti-PD-1 single-agent treatment did not affect the expression of Ki67 in either model. Expression of apoptosis indices significantly increased in the combination treated groups compared to those of controls. Reovirus single agent treatment selectively increased the expression of cleaved-caspase 3 ( $p=0.04$ ) and staining of TUNEL( $p=0.02$ ) in CT26 compared to MC38. While anti-PD-1 administration alone increased TUNEL staining in both models, cleaved-caspase 3 expression significantly increased only in CT26 ( $p=0.04$ ). Although increased evidence was noticed in CT26, combination treatment had profoundly increased the expression of these markers in both models. Ki67



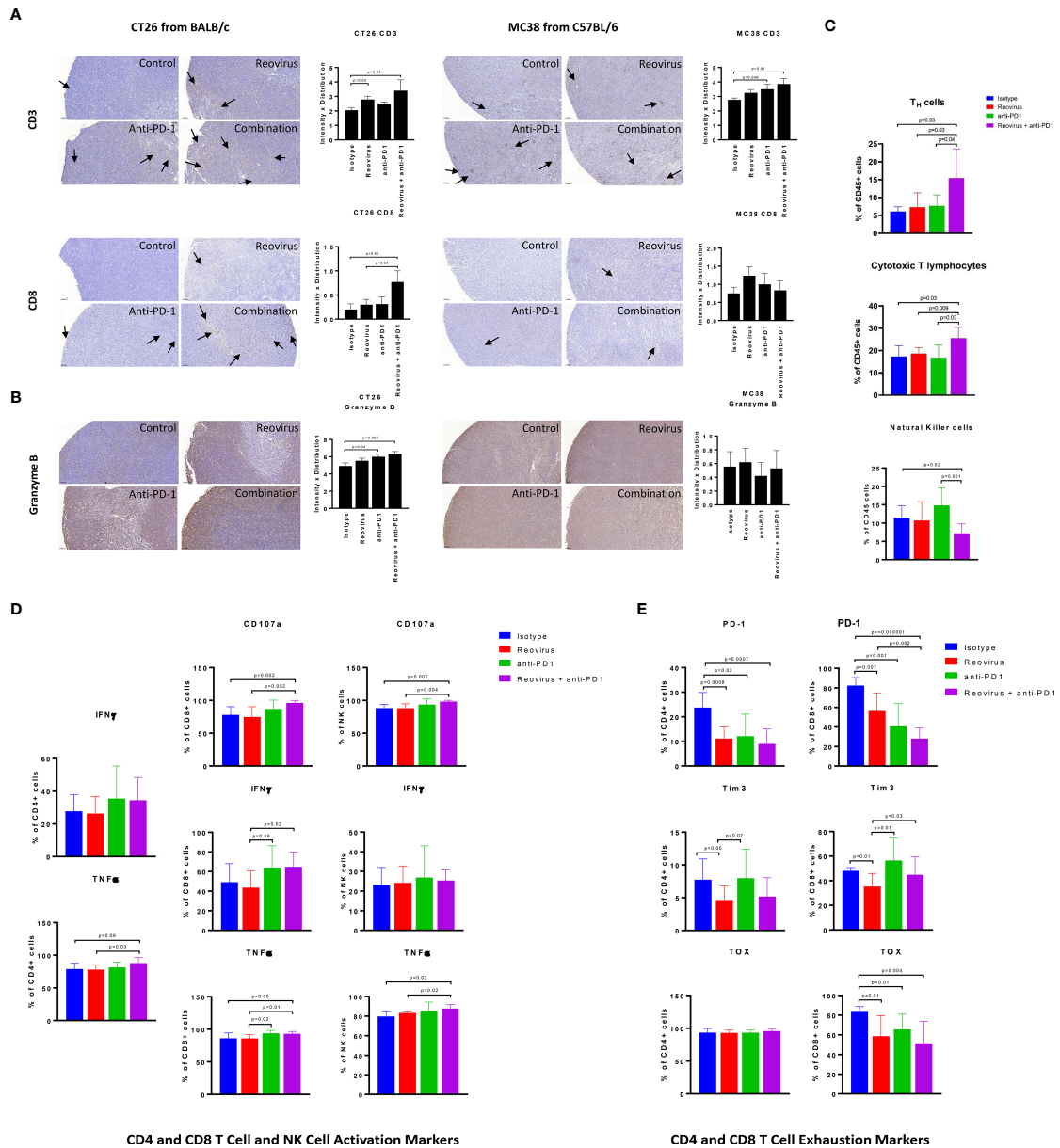


**FIGURE 6**  
 Difference in localization, distribution and expression of cell surface and activation/exhaustion markers in CD4<sup>+</sup> and CD8<sup>+</sup> T cell populations upon reovirus and anti-PD-1 treatment. **(A)** Reovirus in CT26, anti-PD1 in MC38, the combination treatment in both models increased the expression of CD3 (p=NS vs control). While overall, weak distribution, CD8<sup>+</sup> T cell staining was increased upon reovirus (p=0.04) and combination treatment (p=0.03) specifically in CT26. **(B)** Granzyme B, which is a functional marker of NK cells also, increased upon treating with reovirus (p=NS) and combination (p=0.03) in CT26. Overall granzyme B distribution, while high, we didn't observe any significant difference among groups in MC38. **(C)** While single agent treatments displayed insignificant role, combo increased CD4<sup>+</sup> and CD8<sup>+</sup>, and reduced NK cells among overall CD45<sup>+</sup> cell populations in CT26. Strikingly enough, the increment among NK cells boosted by anti-PD-1 abrogated by reovirus administration (p=NS with reovirus). **(D)** Despite overall activation of CD4<sup>+</sup> and CD8<sup>+</sup> T cells, significantly increased expression of surface markers (CD107a, IFN- $\gamma$  and TNF- $\alpha$ ) observed only among CD8<sup>+</sup> cells upon treatment with reovirus plus anti-PD-1. Anti-PD-1 single agent treatment seemingly increasing the expression of all markers, except TNF- $\alpha$  in CD4<sup>+</sup> T cells. While anti-PD-1 alone increased CD107a, IFN- $\gamma$  and TNF- $\alpha$  expression (p=NS) among NK cells, combination treatment significantly increased only CD107a. Reovirus treatment didn't make differences in expression in any of the cytokines studied among NK cell populations. **(E)** Single agents and combination treatment largely reduced the expression of exhaustion markers, however, CD4<sup>+</sup> TOX among all groups and Tim3 among CD4<sup>+</sup> and CD8<sup>+</sup> T cells after anti-PD-1 treatment. Noticeably, Tim3 expression among CD8<sup>+</sup> T cells were increased upon anti-PD-1 treatment.

staining was distributed unevenly across all samples and conditions. The distribution of apoptotic marker was more specific to tumor-rich areas in CT26, whereas it was widespread and unevenly dispersed in MC38 under the combination treatment.

## Alterations in PD-L1/PD-1 axis by reovirus and anti-PD-1 treatment in CT26 but not in MC38 tumors

To examine whether treatment with anti-PD-1 alone or in combination with reovirus impacted the PD-1/PD-L1 axis, we studied the expression of PD-1 and PD-L1 in the resected tumors. In addition to flow cytometry, despite increasing evidence of the presence on cancer/epithelial and immune cell surfaces, we checked the expression of PD-L1 and PD-1 on whole tumor lysates (pooled and individually) and sections using Western blotting and IF respectively. Expression of PD-L1, the key ligand of PD-1, was significantly increased upon reovirus and reovirus plus anti-PD-1 administration ( $p=0.03$ ;  $n=5$ ) in CT26 tumors. MC38 tumors had reduced expression of PD-L1 under all treatment condition. While anti-PD-1 administration reduced the expression of PD-1 protein in both CT26 and MC38 tumors, only CT26 had further reduction upon combining with reovirus ( $p=0.01$ ;  $n=5$ ). Indeed, reovirus single agent and combination groups had increased expression of PD-1 in MC38 (Figure 5A for pooled and Figure 5B and Supplementary Figures 6A, B for individual sample analysis).

SHP-2, the protein tyrosine phosphatase that mediates the negative costimulatory role of PD-1, was also reduced by the absence of PD-1 in CT26 tumors under reovirus, anti-PD-1 and combination administration ( $p<0.05$ ). SHP-2 levels went up by all treatments, particularly, by anti-PD-1 treatment in MC38. Interestingly, NFATc2, one of the transcription factors activated by T cell receptor stimulation increased upon treatment with reovirus and its combination with PD-1 in CT26 tumors ( $p=0.03$ ). There was no change in expression of NFATc2 observed under any treatment conditions in MC38 tumors (Figure 5C). In summary these studies reveal differential activation of PD-L1/PD-1 signaling in the TME of CT26 and MC38 tumors upon treatment with reovirus and anti-PD-1.

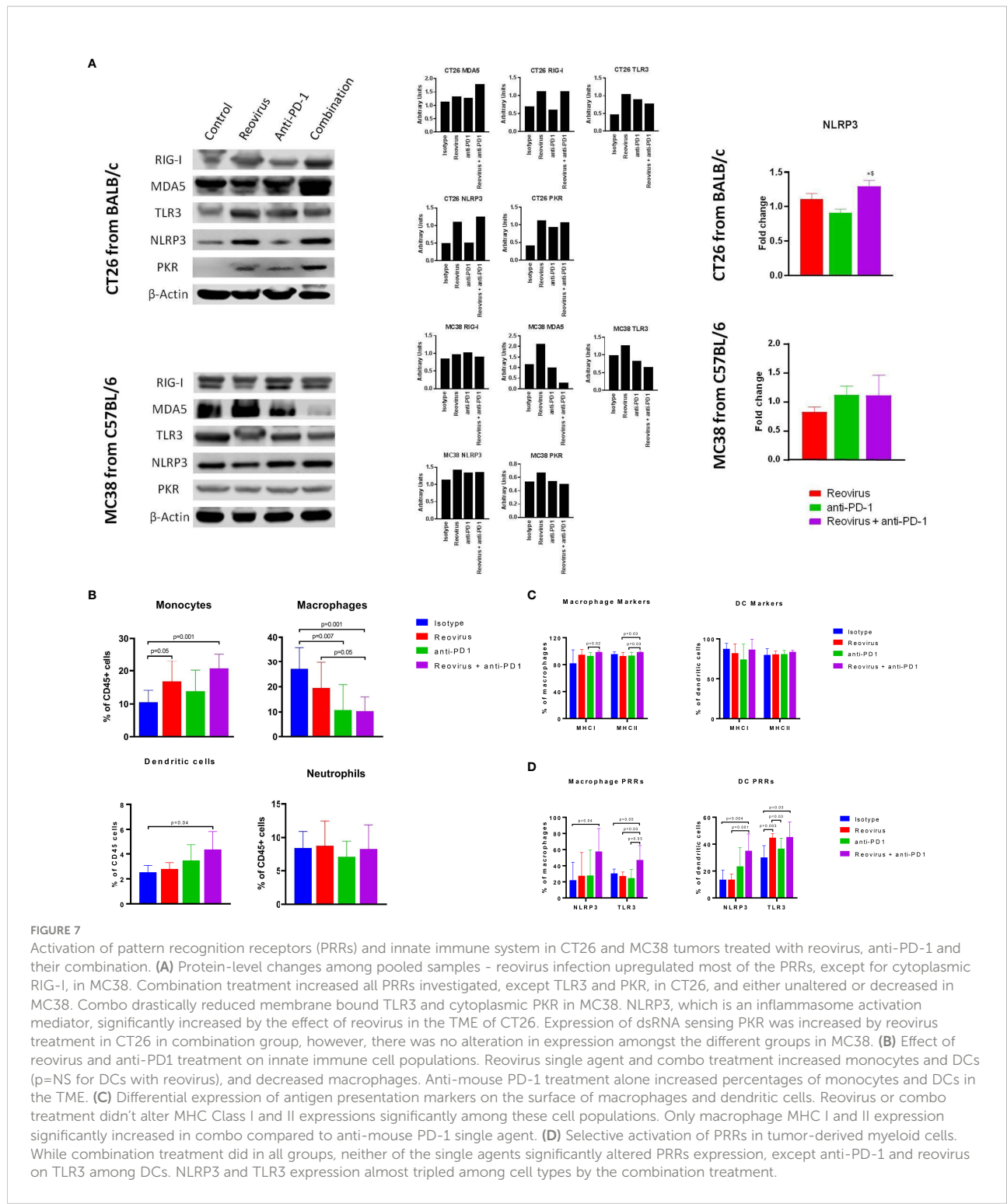
## Reovirus and anti-PD-1 combination therapy synergistically enhances the anti-tumor adaptive immune response in CT26 mouse tumors

Next, we analyzed the composition and activation status of tumor-infiltrating immune cells in the CT26 and MC38 models

treated with this combination. We observed increased T cell infiltration in both MC38 and CT26 tumors treated with anti-PD-1 or reovirus alone, with a further increase in tumors treated with the combination (Figure 6A, top). Similarly, TILs were increased in CT26 tumors treated with anti-PD-1 or reovirus alone and further increased by the combination therapy. In contrast, TILs weren't significantly different among MC38 tumors under any treatment modality (Figure 6A, bottom). Lastly, the combination therapy increased granzyme B expression more than either monotherapy in CT26 tumors, whereas this synergistic response was not seen in MC38 tumors (Figure 6B). This indicates that anti-PD-1 and reovirus combination therapy enhances a cytotoxic immune response in the MSS CT26 model to a greater degree than either monotherapy.

To obtain a more detailed and comprehensive view of the TME in the CT26 model, we enzymatically dissociated the tumors and performed flow cytometric analysis. Consistent with our findings obtained by IHC staining (Figure 6A), we found that the combination treatment synergistically enhanced the infiltration of both  $CD4^+$  ( $p=0.01$ ) and  $CD8^+$  T ( $p=0.02$ ) cells (Figure 6C). We did observe a relative decrease in the proportion of  $CD49b^+$  NK cells (Figure 6C), although this is likely due to the increased proportions of T cells, DCs, and monocytes in these tumor microenvironments (Figure 7B). We next analyzed the functional state of the tumor-infiltrating T cells and NK cells. We found that the combination treatment increased the intracellular expression of the inflammatory cytokines IFN- $\gamma$  and TNF- $\alpha$ , as well as the cytotoxicity marker CD107a in  $CD8^+$  T cells, whereas anti-PD-1 or reovirus monotherapy did not notably increase these markers (Figure 6D). Likewise, the combination therapy also increased the expression of TNF- $\alpha$  in  $CD4^+$  T cells as compared to either monotherapy, although it did not have a marked effect on IFN- $\gamma$  in these cells. The combination treatment also enhanced cytotoxicity and TNF- $\alpha$  expression in NK cells (Figure 6D). The increased expression of TNF- $\alpha$  in  $CD4^+$  T cells was also compounded with a significant decrease in the expression of inhibitory cytokine TGF- $\beta$  in the combinatorial treatment of CT26 tumor cells when compared to single agents further confirming the immune stimulation (Supplementary Figure 5).

As  $CD8^+$  T cells encounter persistent stimulation and immunosuppressive signals in the TME, they can acquire a dysfunctional or "exhausted" state (35). Anti-PD-1 therapy has been reported to relieve T cell exhaustion (36), therefore we hypothesized that combination therapy with reovirus would synergistically decrease T cell exhaustion in infiltrating TILs. To analyze T cell exhaustion, we analyzed the proportion of T cells that expressed the exhaustion markers PD-1 and Tim-3, as well as the transcription factor TOX that has been recently reported to be a specific marker for terminal exhaustion in  $CD8^+$  T cells. Intriguingly, we found that the combination therapy potentially reduced T cell exhaustion in  $CD8^+$  T cells, as



seen by reductions in both PD-1 and TOX expression (Figure 6E). Although significance was not reached, the regulatory T cell (Treg) population was reduced in the combination group as compared to the anti-PD1 further indicating immune activation (Supplementary Figure 5).

Collectively, our data show that reovirus and anti-PD-1 combination therapy synergistically promotes CD8<sup>+</sup> and CD4<sup>+</sup> T cell infiltration, enhances inflammatory and cytotoxic effector functions, and reduces CD8<sup>+</sup> T cell exhaustion.

## Selective activation of pattern recognition receptors (PRRs) and expression of antigen presentation markers of innate immune cell types by reovirus and anti-PD-1 combination

Activation of innate immune cells, particularly antigen-presenting cells such as dendritic cells and macrophages, are key to an effective anti-tumor immune response. We hypothesized that reovirus infection would promote the activation of innate immune pathways through PRR pathways. Sensing of the dsRNA that is produced as a replicative intermediate during reovirus infection and is done by host PRRs such as retinoic acid-inducible gene I (RIG-I), melanoma differentiation-associated protein 5 (MDA-5), toll-like receptor 3 (TLR3) and NOD-like receptor protein 3 (NLRP3) leading to the induction of the innate immune response *via* the type I interferon pathway (37). The effects of reovirus or anti-PD-1 therapy on PRRs was studied in CT26 and MC38 tumors by Western blotting (individual and pooled samples) and qPCR (Figure 7A; Supplementary Figures 6A, B). Cytoplasmic PRRs such as RIG-I and MDA5 and endoplasmic or plasma membrane-bound TLR3 were increased in CT26, and unaltered or decreased in MC38 - particularly, MDA5 - after treatment with reovirus and anti-PD-1. TLR3, NLRP3 (inflammasome mediator PRR), and protein kinase R (PKR; cytoplasmic sensor of viral-mediated dsRNA) were upregulated under both single agent reovirus- and combination-treated groups in CT26, however, the changes were insignificant in MC38 ( $p > 0.05$ ). Notably, the increased expression of RIG-I, MDA5, PKR, and NLRP3 was greatest in the combination treatment group, suggesting a synergistic increase in the activation of innate immune pathways. We further confirmed the increased expression of NLRP3 at the mRNA level with qPCR (Figure 7A, right).

To further analyze the composition of the tumor-infiltrating myeloid cells, we performed flow cytometric analysis of dissociated tumors. We found that the combination treatment significantly decreased the populations of CD11b<sup>+</sup> F4/80<sup>+</sup> macrophages, which are a major population of immunosuppressive cells in the TME. In contrast, the combination treatment increased the populations of Ly6C<sup>+</sup> monocytes and CD11c<sup>+</sup> dendritic cells (DCs). No significant changes were seen in the Ly6G<sup>+</sup> neutrophil population in any treatment group (Figure 7B). Next, we sought to analyze the expression of activation markers and PRRs in the myeloid cells. The expression of antigen-presentation molecules MHC I and MHC II on macrophages and DCs was high at baseline (18) even in the isotype-treated group and was not significantly increased with treatment (Figure 7C). Interestingly, expression of the PRRs such as NLRP3 and TLR3 was increased with combination treatment in both macrophages and DCs (Figure 7D). This

indicates that the increased expression of PRRs seen with Western blotting was at least in part due to the contribution of tumor-infiltrating myeloid cells. Put together, our studies show that combination of reovirus and anti-PD-1 treatment synergistically activates innate immune PRR pathways, reduces immunosuppressive macrophage populations while promoting effector monocyte and DC populations, and increases the expression of PRR molecules within both macrophages and DCs.

## Discussion

The KEYNOTE-016 trial that evaluated pembrolizumab monotherapy, and CheckMate-142 trial which evaluated nivolumab plus ipilimumab examined the response of MSI mCRC to immunotherapy. The KEYNOTE-016 also included a subset of patients with MSS mCRC (38, 39). In contrast to the positive results observed in MSI tumors, MSS mCRC patients did not respond to checkpoint inhibition, highlighting the predictive value of microsatellite instability in response to immunotherapy in mCRC. Thus, it is of critical importance to find strategies to improve the response of immune cold tumors to ICI. Here, we demonstrate the feasibility and efficacy of using oncolytic reovirus therapy alongside anti-PD-1 treatment as a novel combination treatment strategy for MSS CRC tumors.

By studying the expression of key genes related to immune regulation, microarray and computational analysis of global immune-response genes in *in vitro* models, we highlight the *in vitro* first-in-class discovery that the inherent MMR status (MSI or MSS) is a critically important determinant of sensitivity to reovirus infection. This prompted us to formulate the hypothesis that a combination of reovirus with an ICI, such as an anti-PD-1, would have synergistic therapeutic efficacy against MSS type of CRC tumors. Oncolytic viruses along with immune-modulating agents have shown to be increasingly effective previously too. Heavily pretreated CRC patients were administered the oncolytic vaccinia virus Pexa-Vec [JX-594] engineered to express GM-CSF, a hematopoietic growth factor that increases dendritic cell differentiation, maturation and function and induced tumor reactive T cells and reached stable disease in 67% ( $n = 10$ ) of patients (40, 41). The biweekly injection did not lead to dose-limiting toxicities in this phase Ib study alone (41) or in a phase I/II study in combination with checkpoint inhibitors tremelimumab (CTLA-4) and durvalumab (PD-L1) (42). A phase Ib trial testing the combination of T-VEC and pembrolizumab revealed a high overall response rate (ORR) of 62% and complete responses in 33% of melanoma patients independent of baseline CD8<sup>+</sup> infiltration (43). Few challenges that were encountered include optimizing tumor tropism, viral delivery, and enhancing anti-tumor immunity.

We demonstrate that the antitumor activity of the drug combination is associated with the induction of

apoptosis in tumor cells as well as immune activation in the microenvironment. With regards to the former, our time-lapse live-cell imaging and IHC data indicate that combinatorial treatment reduced the expression of Ki67 while enhancing the expression of cleaved-caspase3 and TUNEL staining. Our group and others have demonstrated that defective activation of the antiviral PKR-eIF2 $\alpha$  pathway is a key determinant of direct oncolysis initiated by reovirus infection (10, 17, 44, 45), enabling efficient viral replication, and immune activation in a later stage (22). Reovirus infection also triggers the cellular interferon (IFN) response to produce Type 1 IFN's alpha and beta (IFN $\alpha/\beta$ ). Secreted IFN $\alpha/\beta$  can stimulate the JAK-STAT pathway in an autocrine or paracrine manner to activate hundreds of IFN-stimulated genes (ISGs), many of which have antiviral activities that elicit an antiviral state (46).

Activation of immune response KEGG pathways such as, TNF-, NOD-like receptor-, or NF- $\kappa$ B-signaling following reovirus treatment could then further enhance the activity of this combination by enhancing immune-mediated cell killing, as observed in the co-culture system (28, 47, 48). In addition to these pathways, other pathways may also be involved. For example, we observed that reovirus treatment increased expression of CREB1 in both MSI/MSS and *KRAS*<sup>Mut</sup>/*KRAS*<sup>Wt</sup> cell lines indicating an altered cell death signaling and viral immune mediation (49). CREB1 has been shown to play a large role in TNF signaling pathways (50), raising the possibility that reovirus treatment may increase TNF signaling within CRC tumors, leading to apoptosis and total cell death (51). Combination of agents that increase the expression of death receptor 5 (DR5) and its ligand, TNF-related apoptosis-inducing ligand (TRAIL), is a novel anti-CRC therapy, and correlate with tumor regression (52). Alongside reovirus treatment, TNF signaling upregulation secondary to CREB1 expression may prove efficacious to CRC treatment in future studies. Targeting CREB1 binding protein/ $\beta$ -catenin, combined with PD-1/PD-L1 blockade, has shown potential as a new therapeutic strategy for treating liver metastasis in CRC (53). Further studies are needed on the role of CREB1 and TNF signaling in MSS cancers and their susceptibility to immunotherapy.

Consideration of treatment regimens will be particularly important for combination of reovirus with ICIs because anti-CTLA-4 antibodies are likely to potentiate early stages of T cell priming, whilst anti-PD1/anti-PD-L1 mAbs would act to reverse T cell exhaustion within the TME (54). In a recent combinatorial study, reovirus-specific – but, not tumor-specific – CD8<sup>+</sup> TILs served as non-exhausted effector cells for the subsequently systemically administered CD3-bispecific antibodies (55). Oncolytic virus (OV)-infected cancer cells tend to down-regulate their class I MHC making themselves a good target for functionally active CD107a<sup>+</sup> NK cells. Although NK cells may kill infected cancer cells and limit the amplification of OVs, studies have found that NK cells often have positive effects on therapeutic outcomes of OVs (56, 57). Proving the oncolytic

nature of reovirus and its influence on immune response mediators such as cytokines and cellular regulators are important in determining its possibility to combine with an ICI to test synergistic efficacy. The activation of innate-sensing pathways of antigen-presenting CD11c<sup>+</sup> DCs, CD11b<sup>+</sup> macrophages and monocytes within TME may trigger enhanced CD8<sup>+</sup> T cell responses against the tumor (58).

OVs promote PD-L1 expression in both cancer and TME cells and by combining with an anti-PD-L1 antibody this barrier can be effectively overcome (59). Increased effect of reovirus by anti-PD-1 treatment was analyzed using double-stranded RNA-dependent kinase - PKR - that induces inflammation by regulating the expression of the NLR family pyrin domain-containing 3 inflammasome – NLRP3 - through NF- $\kappa$ B signaling. NLRP3 and TLR3 sense a wide range of pathogen-associated molecular patterns (PAMPs) and damage-associated molecular patterns (DAMPs) (60). We observed an increase in the expression of NLRP3 in CT26 CRC TME which corroborates and augments the previously published findings regarding the function of NLRP3. APCs expressing PRRs such as TLR3, MDA5, RIG-I, NLRP3 etc. can be directly activated by PAMPs or DAMPs to become competent to prime T cell responses (37). Engagement of PRRs on DCs induces NF- $\kappa$ B activation, up-regulation of co-stimulatory molecules, and production of cytokines and promotion of cross-priming (61). PAMPs and DAMPs can also be produced by immunogenic cell death (ICD) of tumor cells induced by reovirus. We are thus confident that reovirus and anti-PD-1 antibody combination is a promising therapeutic approach to convert cold MSS tumors to inflamed immune therapy sensitive tumors. Thus, reovirus promotes an overall inflammatory TME and increases the responsiveness of MSS tumors to immunotherapy (62).

This study has certain limitations deserving of discussion. Conceptually, converting “cold tumors” to “hot tumors” using various mechanisms have been attempted for many years, with limited success. Concomitant therapies such as cytotoxic chemotherapy, targeted biologic therapy, immune mechanisms unrelated to the PD-1/PD-L1 axis, biologic agents, and radiation have all been attempted in several scenarios. To date, few approaches have found clinical success to meet the rigor of USFDA approval – such as the use of the anti VEGF agent lenvatinib (in combination with pembrolizumab in patients with renal (63) and endometrial cancer (64), and bevacizumab (with atezolizumab for patients with hepatocellular cancer (65). More recently the combination of an anti-LAG-3 antibody with nivolumab for use in patients with melanoma (66) added new hopes to this approach. However, to date, no infectious agent has garnered robust clinical data to justify its use in patients, concomitant with immune therapy.

Translating pre-clinical findings to the clinic remains a formidable challenge. Despite tremendous effort and infallible scientific rationale for clinical studies, most clinical trials fail to recapitulate the pre-clinical activity of these interventions.

While our study may have similar limitations, there is patient experience on the combination of reovirus with pembrolizumab [in pancreatic cancer (67)], with at least the supporting data for immune changes in the tumor microenvironment similar to our *in vivo* models. In our present study, we were restricted to 2 syngeneic murine models to test the efficacy of the combination, i.e., Kras<sup>Mut</sup> MSS and Kras<sup>WT</sup> MSI colorectal cancer. Further studies in other models are warranted, for example to examine combinatorial effect in a Kras<sup>Mut</sup> MSI and conversely, in a Kras<sup>WT</sup> MSS syngeneic mouse model.

Further, we were limited in our ability to comprehensively evaluate the changes in gene expression under various conditions of intervention. Microarray is a powerful tool to evaluate changes at the genetic level but is also limited by prohibitive costs. We aim to continue this approach in later studies with more resources and funding availability. Similarly, we will also encourage the study of T cell response with in-depth immune cell profiling and T cell characterization, such as T-bet, GATA3, ROR $\gamma$ -t and Bcl6 based Th1, Th2, Th17 and Tfh classification of CD4 T cells (68), including T cell receptor studies.

Herein we report for the first time that immune-insensitive MSS tumors that account for 85% of all CRC can be effectively converted to immunotherapy-sensitive cancers by introducing reovirus to the therapeutic regimen. Our data confidently establishes that reovirus sensitizes MSS tumors to anti-PD-1 therapy *via* increasing the expression of PD-L1 marker on respective target cells. The combinatorial treatment has successfully immune populated the MSS tumor TME in all three study models. Immunotherapy, which has achieved phenomenal success in many cancer types, may now be successfully implemented in MSS 'cold' or immunosuppressive CRC tumors, and provides a rationale to extend combination reovirus-ICI therapy into clinical testing.

## Data availability statement

The original contributions presented in the study are included in the article/[Supplementary Material](#). Further inquiries can be directed to the corresponding author.

## Ethics statement

The animal study was reviewed and approved by Institutional Animal Care and Use Committee (IACUC), Albert Einstein College of Medicine, New York USA.

## Author contributions

TA, conceptualization, supervision, resources, methodology, investigation, analysis, and writing the original draft. PJ,

methodology, investigation, formal analysis, validation, data curation, and writing in-part. TF, methodology, investigation, formal analysis, software, and writing in-part. JJ and CD, methodology, investigation and formal analysis. HG, methodology, investigation, and visualization. RiM and RG, formal analysis, and investigation. JM and XZ, supervision, methodology, analysis and editing. RaM, data curation, supervision, methodology, analysis, and editing. SG, conceptualization, resources, data curation, software, formal analysis, supervision, funding acquisition, validation, methodology, project administration, and editing. All authors contributed to the article and approved the submitted version.

## Funding

SG was supported by NIH/AG1R21 NIH grant AG1R21AG058027-01. RaM was supported by Yeshiva University startup fund 2A4108.

## Acknowledgments

We gratefully acknowledge the Office of Grant Support, Genomic Facility, Flow Cytometry Core Facility, and the Analytical Imaging Facility of Albert Einstein College of Medicine along with the NCI cancer center support grant (P30CA013330), which partially supports all morphometric work conducted with 3D Histech P250 High-Capacity Slide Scanner SIG #1S10OD019961-01 of the shared facilities. We also thankfully acknowledge Dr. Lidija Klampfer of Southern Research Institute, Birmingham, Alabama for the kind gift of Hke3 cell line.

## Conflict of interest

The authors declare that the research was conducted in the absence of any commercial or financial relationships that could be construed as a potential conflict of interest.

## Publisher's note

All claims expressed in this article are solely those of the authors and do not necessarily represent those of their affiliated organizations, or those of the publisher, the editors and the reviewers. Any product that may be evaluated in this article, or claim that may be made by its manufacturer, is not guaranteed or endorsed by the publisher.

## Supplementary material

The Supplementary Material for this article can be found online at: <https://www.frontiersin.org/articles/10.3389/fonc.2022.1018767/full#supplementary-material>

### SUPPLEMENTARY FIGURE 1

Individual growth arrest pattern of the 13 cell lines upon reovirus treatment. MTT assay revealed that reovirus treatment of 5 MOI for 24 hours induced significant growth arrest in all 13 CRC cell lines studied.

### SUPPLEMENTARY FIGURE 2

Differential expression of global immune response genes under reovirus infection in CRC cell lines categorized on *KRAS* status. **(A)** Hierarchical-clustering profile across differentially expressed genes (DEGs) participating in immune pathways upon treatment with reovirus in *KRAS*<sup>Mut</sup> and *KRAS*<sup>Wt</sup> groups. RMA normalized expression values for the 13 genes were used to generate a heat-map in the TAC software. The colors indicate the expression value relative to the median expression value per gene in the dataset. Red indicates upregulation relative to the median value and green indicates downregulation relative to the median value. **(B)** GO term enrichment and KEGG pathway analyses of DEGs using DAVID. Differentially expressed probes between *KRAS*<sup>Mut</sup> and *KRAS*<sup>Wt</sup> cell lines treated with reovirus were selected based on meeting the criteria of  $p \leq 0.05$ , and divided into positive and negative fold changes lists and used to determine enrichment. **(C)** Protein interaction analysis using STRING. The different colored nodes represent different genes. Different edges (lines) show the interplay between genes. Edge strength is shown by thickness of the line, the thicker the line, the stronger the interaction. Hub networks made using MCODE demonstrate the genes within the PPI that were screened to display the most highly upregulated. The genes not included in the hub networks did not have substantial interaction amongst the other genes in the list, therefore they were not included. **(D)** Venn diagram created using the TAC software. It illustrates the clear point that between the *KRAS* subgroups, CREB1 gene is the only commonality out of 16 genes, 4 in the *KRAS*<sup>Mut</sup> and 12 genes in the *KRAS*<sup>Wt</sup> groups.

### SUPPLEMENTARY FIGURE 3

Classification of 59 CRC cell lines based on expression of stemness markers. Heat-map of stemness and epithelial cell markers' expression among CRC cell lines studied using RNA-Seq. Transcript levels are given as reads per kilobase per million mapped (RPKM) values.

### SUPPLEMENTARY FIGURE 4

Levels of cell death among *KRAS*<sup>Wt</sup> and *KRAS*<sup>Mut</sup> human CRC cell lines co-cultured with human PBMC (*ex vivo*) and treated with reovirus, anti-human PD-1 and their combination. Trends in fold difference and significance are depicted on box and whisker plot. Combination treatment compared to placebo rendered no significance in both the groups ( $p$  values in bold letters indicate significance).

### SUPPLEMENTARY FIGURE 5

Alterations in Treg cell populations and TGF- $\beta$  expression in CD4<sup>+</sup> T cells upon treatment with reovirus and anti-PD-1 on CT26 tumors *in vivo*. While both single agents displayed significant role, combo treatment compared to control kept regulatory T cell levels unaltered. Interestingly enough, while reovirus treatment reduced, anti-PD-1 alone significantly increased Tregs in the TME of CT26. TGF- $\beta$ , an immunosuppressive marker, by following the trends in Tregs was increased by single agent anti-PD-1 treatment. Combo treatment compared to control and single agent reovirus kept TGF- $\beta$  expression unaltered.

### SUPPLEMENTARY FIGURE 6

Protein level expressions of PD-L1, PD-1 and PRRs among individual tumor samples. Reovirus infection in CT26 upregulated most of the PRRs studied and either unaltered or decreased in expression, except for MDA5, in MC38. Cytoplasmic PRRs, RIG-I and MDA5, significantly increased upon combination treatment in CT26, whereas decreased in MC38. Combo treatment significantly increased membrane bound TLR3 in CT26, whereas reduced ( $p=NS$ ) in expression in MC38. NLRP3, which is an inflammasome activation mediator, significantly increased by protein expression in CT26 TME, whereas mostly unaltered under any treatment conditions in MC38. dsRNA-sensing PRR, PKR, significantly increased by combo in CT26, however, reduced in expression in MC38. Densitometry quantifications ( $n=5$ ) are given on bar charts.

### SUPPLEMENTARY TABLE 1

Molecular profiling of key CRC cell lines studied in the manuscript. Summary of microsatellite instability and *KRAS* gene mutation statuses of seven human and two mouse CRC cell lines used in the manuscript.

### SUPPLEMENTARY TABLE 2

List of antibodies and primers used.

### SUPPLEMENTARY TABLE 3

Details of the experimental set-up of *ex vivo* co-culture study. Every group was added with human CRC cell lines and human PBMCs consecutively as part of establishing the culture, and nuclear labeling and dead cell counting reagents for identification and measurement, respectively.

### SUPPLEMENTARY MOVIE

Reovirus and anti-human PD-1 (nivolumab) combinatorial treatment increases cell death among MSS compared to MSI cell line in an *ex vivo* co-culture system. Cytotoxicity of reovirus and anti-human PD-1 treatment towards cell lines was monitored by time-lapse live-cell imaging (Cytotox Red uptake and release) and found that it has significantly increased in HT29 (MSS) cell line. Combo treatment was comparatively ineffective in cell killing in LIM2405 (MSI). Statistical analysis is shown for the 4 hr and 9 hr co-incubation time points. Data represent at least 3 independent experiments ( $n=12$ ). Mean values  $\pm$  SEM are calculated.

## References

- Picard E, Verschoor CP, Ma GW, Pawelec G. Relationships between immune landscapes, genetic subtypes and responses to immunotherapy in colorectal cancer. *Front Immunol* (2020) 11:369. doi: 10.3389/fimmu.2020.00369
- Lengyel CG. Microsatellite instability as a predictor of outcomes in colorectal cancer in the era of immune-checkpoint inhibitors. *Curr Drug Targets* (2021) 22(9):968–76. doi: 10.2174/1389450122666210325121322
- Eso Y, Seno H. Current status of treatment with immune checkpoint inhibitors for gastrointestinal, hepatobiliary, and pancreatic cancers. *Therap Adv Gastroenterol* (2020) 13:1756284820948773. doi: 10.1177/1756284820948773
- Zaravinos A, Roufas C, Nagara M, de Lucas Moreno B, Oblovatskaya M, Efstathiades C, et al. Cytolytic activity correlates with the mutational burden and deregulated expression of immune checkpoints in colorectal cancer. *J Exp Clin Cancer Res* (2019) 38(1):364. doi: 10.1186/s13046-019-1372-z
- Glode AE, May MB. Immune checkpoint inhibitors: Significant advancements in non-small cell lung cancer treatment. *Am J Health Syst Pharm* (2021) 78(9):769–80. doi: 10.1093/ajhp/zxab041
- Gupta R, Sinha S, Paul RN. The impact of microsatellite stability status in colorectal cancer. *Curr Probl Cancer* (2018) 42(6):548–59. doi: 10.1016/j.cupr.2018.06.010

7. Fujiyoshi K, Yamamoto G, Takenoya T, Takahashi A, Arai Y, Yamada M, et al. Metastatic pattern of stage iv colorectal cancer with high-frequency microsatellite instability as a prognostic factor. *Anticancer Res* (2017) 37(1):239–47. doi: 10.21873/anticancerres.11313
8. Maitra R, Augustine T, Dayan Y, Chandy C, Coffey M, Goel S. Toll like receptor 3 as an immunotherapeutic target for kras mutated colorectal cancer. *Oncotarget* (2017) 8(21):35138–53. doi: 10.18632/oncotarget.16812
9. Liu X, Jakubowski M, Hunt JL. Kras gene mutation in colorectal cancer is correlated with increased proliferation and spontaneous apoptosis. *Am J Clin Pathol* (2011) 135(2):245–52. doi: 10.1309/AJCP7FO2VAXIVSTP
10. Maitra R, Ghalib MH, Goel S. Reovirus: A targeted therapeutic—progress and potential. *Mol Cancer Res* (2012) 10(12):1514–25. doi: 10.1158/1541-7786.MCR-12-0157
11. Fountzilias C, Patel S, Mahalingam D. Review: Oncolytic virotherapy, updates and future directions. *Oncotarget* (2017) 8(60):102617–39. doi: 10.18632/oncotarget.18309
12. Saha D, Martuza RL, Rabkin SD. Oncolytic herpes simplex virus immunovirotherapy in combination with immune checkpoint blockade to treat glioblastoma. *Immunotherapy* (2018) 10(9):779–86. doi: 10.2217/imt-2018-0009
13. Jonas BA. Combination of an oncolytic virus with pd-L1 blockade keeps cancer in check. *Sci Transl Med* (2017) 9(386):ean2781. doi: 10.1126/scitranslmed.aan2781
14. John P, Wei Y, Liu W, Du M, Guan F, Zang X. The B7x immune checkpoint pathway: From discovery to clinical trial. *Trends Pharmacol Sci* (2019) 40(11):883–96. doi: 10.1016/j.tips.2019.09.008
15. Augustine T, Maitra R, Zhang J, Nayak J, Goel S. Sensitization of colorectal cancer to irinotecan therapy by parp inhibitor rucaparib. *Invest New Drugs* (2019) 37(5):948–60. doi: 10.1007/s10637-018-00717-9
16. Augustine TA, Maitra R, John P, Goel S. Potentiating effect of reovirus in anti-Pd1 therapy in colorectal cancer. *Cancer Res* (2018) 78(13):3917. doi: 10.1158/1538-7445.Am2018-3917
17. Maitra R, Seetharam R, Tesfa L, Augustine TA, Klampfer L, Coffey MC, et al. Oncolytic reovirus preferentially induces apoptosis in kras mutant colorectal cancer cells, and synergizes with irinotecan. *Oncotarget* (2014) 5(9):2807–19. doi: 10.18632/oncotarget.1921
18. Ohaegbulam KC, Liu W, Jeon H, Almo SC, Zang X. Tumor-expressed immune checkpoint B7x promotes cancer progression and antigen-specific Cd8 T cell exhaustion and suppressive innate immune cells. *Oncotarget* (2017) 8(47):82740–53. doi: 10.18632/oncotarget.21098
19. Staats J. Immunophenotyping of human regulatory T cells. *Methods Mol Biol* (2019) 2032:141–77. doi: 10.1007/978-1-4939-9650-6\_9
20. Atzmon G, Yang XM, Muzumdar R, Ma XH, Gabriely I, Barzilai N. Differential gene expression between visceral and subcutaneous fat depots. *Horm Metab Res* (2002) 34(11–12):622–8. doi: 10.1055/s-2002-38250
21. Maitra R, Fogel E, Parakrama R, Goel S. Molecular tools for metastatic colorectal cancer characterization. *J Cell Immunol* (2020) 2(6):359–63. doi: 10.33696/immunology.2.067
22. Parakrama R, Fogel E, Chandy C, Augustine T, Coffey M, Tesfa L, et al. Immune characterization of metastatic colorectal cancer patients post reovirus administration. *BMC Cancer* (2020) 20(1):569. doi: 10.1186/s12885-020-07038-2
23. Yu H, Pei D, Chen L, Zhou X, Zhu H. Identification of key genes and molecular mechanisms associated with dedifferentiated liposarcoma based on bioinformatic methods. *Onco Targets Ther* (2017) 10:3017–27. doi: 10.2147/OTT.S132071
24. Mouradov D, Sloggett C, Jorissen RN, Love CG, Li S, Burgess AW, et al. Colorectal cancer cell lines are representative models of the main molecular subtypes of primary cancer. *Cancer Res* (2014) 74(12):3238–47. doi: 10.1158/0008-5472.CAN-14-0013
25. Chisanga D, Keerthikumar S, Pathan M, Ariyaratne D, Kalra H, Boukouris S, et al. Colorectal cancer atlas: An integrative resource for genomic and proteomic annotations from colorectal cancer cell lines and tissues. *Nucleic Acids Res* (2016) 44(D1):D969–74. doi: 10.1093/nar/gkv1097
26. Wang J, Mouradov D, Wang X, Jorissen RN, Chambers MC, Zimmerman LJ, et al. Colorectal cancer cell line proteomes are representative of primary tumors and predict drug sensitivity. *Gastroenterology* (2017) 153(4):1082–95. doi: 10.1053/j.gastro.2017.06.008
27. BioScience E *Live-cell analysis inside your incubator. incucyte S3 live-cell analysis system. manufacturer's brochure* (2018). Ann Arbor, MI: Essen BioScience. Available at: [https://www.essenbioscience.com/media/uploads/files/8000-0529-B00-IncuCyte\\_S3\\_Brochure.pdf](https://www.essenbioscience.com/media/uploads/files/8000-0529-B00-IncuCyte_S3_Brochure.pdf) (Accessed 6 December 2018).
28. Thirukkumaran CM, Shi ZQ, Luider J, Kopciuk K, Gao H, Bahlis N, et al. Reovirus modulates autophagy during oncolysis of multiple myeloma. *Autophagy* (2013) 9(3):413–4. doi: 10.4161/auto.22867
29. Serguienko A, Wang MY, Myklebost O. Real-time vital mineralization detection and quantification during in vitro osteoblast differentiation. *Biol Proced Online* (2018) 20:14. doi: 10.1186/s12575-018-0079-4
30. Lee KH, Min HS, Han SW, Oh DY, Lee SH, Kim DW, et al. Erccl expression by immunohistochemistry and egfr mutations in resected non-small cell lung cancer. *Lung Cancer* (2008) 60(3):401–7. doi: 10.1016/j.lungcan.2007.10.014
31. Odell ID, Cook D. Immunofluorescence techniques. *J Invest Dermatol* (2013) 133(1):e4. doi: 10.1038/jid.2012.455
32. Lee C, Do HTT, Her J, Kim Y, Seo D, Rhee I. Inflammasome as a promising therapeutic target for cancer. *Life Sci* (2019) 231:116593. doi: 10.1016/j.lfs.2019.116593
33. Toffalori C, Zito L, Gambacorta V, Riba M, Oliveira G, Bucci G, et al. Immune signature drives leukemia escape and relapse after hematopoietic cell transplantation. *Nat Med* (2019) 25(4):603–11. doi: 10.1038/s41591-019-0400-z
34. Wahab SMR, Islam F, Gopalan V, Lam AK. The identifications and clinical implications of cancer stem cells in colorectal cancer. *Clin Colorectal Cancer* (2017) 16(2):93–102. doi: 10.1016/j.clcc.2017.01.011
35. McLane LM, Abdel-Hakeem MS, Wherry EJ. Cd8 T cell exhaustion during chronic viral infection and cancer. *Annu Rev Immunol* (2019) 37:457–95. doi: 10.1146/annurev-immunol-041015-055318
36. Miller BC, Sen DR, Al Abosy R, Bi K, Virkud YV, LaFleur MW, et al. Subsets of exhausted Cd8(+) T cells differentially mediate tumor control and respond to checkpoint blockade. *Nat Immunol* (2019) 20(3):326–36. doi: 10.1038/s41590-019-0312-6
37. Husser L, Alves MP, Ruggli N, Summerfield A. Identification of the role of rig-I, mda-5 and Tlr3 in sensing rna viruses in porcine epithelial cells using lentivirus-driven rna interference. *Virus Res* (2011) 159(1):9–16. doi: 10.1016/j.virusres.2011.04.005
38. Le DT, Durham JN, Smith KN, Wang H, Bartlett BR, Aulakh LK, et al. Mismatch repair deficiency predicts response of solid tumors to pd-1 blockade. *Science* (2017) 357(6349):409–13. doi: 10.1126/science.aan6733
39. Overman MJ, McDermott R, Leach JL, Lonardi S, Lenz HJ, Morse MA, et al. Nivolumab in patients with metastatic DNA mismatch repair-deficient or microsatellite instability-high colorectal cancer (Checkmate 142): An open-label, multicentre, phase 2 study. *Lancet Oncol* (2017) 18(9):1182–91. doi: 10.1016/S1470-2045(17)30422-9
40. de Graaf JF, de Vor L, Fouchier RAM, van den Hoogen BG. Armed oncolytic viruses: A kick-start for anti-tumor immunity. *Cytokine Growth Factor Rev* (2018) 41:28–39. doi: 10.1016/j.cytogfr.2018.03.006
41. Park SH, Breitbach CJ, Lee J, Park JO, Lim HY, Kang WK, et al. Phase 1b trial of biweekly intravenous pexa-vec (Jx-594), an oncolytic and immunotherapeutic vaccinia virus in colorectal cancer. *Mol Ther* (2015) 23(9):1532–40. doi: 10.1038/mt.2015.109
42. Hwang JK, Hong J, Yun CO. Oncolytic viruses and immune checkpoint inhibitors: Preclinical developments to clinical trials. *Int J Mol Sci* (2020) 21(22):8627. doi: 10.3390/ijms21228627
43. Ribas A, Dummer R, Puzanov I, VanderWalde A, Andtbacka RHI, Michielin O, et al. Oncolytic virotherapy promotes intratumoral T cell infiltration and improves anti-Pd-1 immunotherapy. *Cell* (2017) 170(6):1109–19 e10. doi: 10.1016/j.cell.2017.08.027
44. McLaughlin M, Pedersen M, Roulstone V, Bergerhoff KF, Smith HG, Whittock H, et al. The perk inhibitor Gsk2606414 enhances reovirus infection in head and neck squamous cell carcinoma *Via* an Atf4-dependent mechanism. *Mol Ther Oncol* (2020) 16:238–49. doi: 10.1016/j.omto.2020.01.001
45. Villalona-Calero MA, Lam E, Otterson GA, Zhao W, Timmons M, Subramaniam D, et al. Oncolytic reovirus in combination with chemotherapy in metastatic or recurrent non-small cell lung cancer patients with kras-activated tumors. *Cancer* (2016) 122(6):875–83. doi: 10.1002/cncr.29856
46. Barragan-Iglesias P, Franco-Enzastiga U, Jeevakumar V, Shiers S, Wangzhou A, Granados-Soto V, et al. Type I interferons act directly on nociceptors to produce pain sensitization: Implications for viral infection-induced pain. *J Neurosci* (2020) 40(18):3517–32. doi: 10.1523/JNEUROSCI.3055-19.2020
47. Kyula JN, Khan AA, Mansfield D, Karapanagiotou EM, McLaughlin M, Roulstone V, et al. Synergistic cytotoxicity of radiation and oncolytic Lister strain vaccinia in (V600d/E)Braf mutant melanoma depends on jnk and tnf-alpha signaling. *Oncogene* (2014) 33(13):1700–12. doi: 10.1038/onc.2013.112
48. Shulak L, Beljanski V, Chiang C, Dutta SM, Van Grevenynghe J, Belgnaoui SM, et al. Histone deacetylase inhibitors potentiate vesicular stomatitis virus oncolysis in prostate cancer cells by modulating nf-kappab-Dependent autophagy. *J Virol* (2014) 88(5):2927–40. doi: 10.1128/JVI.03406-13
49. Xiao X, Li BX, Mitton B, Ikeda A, Sakamoto KM. Targeting creb for cancer therapy: Friend or foe. *Curr Cancer Drug Targets* (2010) 10(4):384–91. doi: 10.2174/156800910791208535
50. Du Y, Teng X, Wang N, Zhang X, Chen J, Ding P, et al. Nf-kappab and enhancer-binding creb protein scaffolded by creb-binding protein (Cbp)/P300

proteins regulate Cd59 protein expression to protect cells from complement attack. *J Biol Chem* (2014) 289(5):2711–24. doi: 10.1074/jbc.M113.525501

51. Errington F, Steele L, Prestwich R, Harrington KJ, Pandha HS, Vidal L, et al. Reovirus activates human dendritic cells to promote innate antitumor immunity. *J Immunol* (2008) 180(9):6018–26. doi: 10.4049/jimmunol.180.9.6018
52. Edagawa M, Kawauchi J, Hirata M, Goshima H, Inoue M, Okamoto T, et al. Role of activating transcription factor 3 (Atf3) in endoplasmic reticulum (Er) stress-induced sensitization of P53-deficient human colon cancer cells to tumor necrosis factor (Tnf)-related apoptosis-inducing ligand (Trail)-mediated apoptosis through up-regulation of death receptor 5 (Dr5) by zerumbone and celecoxib. *J Biol Chem* (2014) 289(31):21544–61. doi: 10.1074/jbc.M114.558890
53. Osawa Y, Kojika E, Nishikawa K, Kimura M, Osakaya S, Miyauchi H, et al. Programmed cell death ligand 1 (Pd-L1) blockade attenuates metastatic colon cancer growth in camp-response element-binding protein (Creb)-binding protein (Cbp)/Beta-catenin inhibitor-treated livers. *Oncotarget* (2019) 10(32):3013–26. doi: 10.18632/oncotarget.26892
54. Muller L, Berkeley R, Barr T, Ilett E, Errington-Mais F. Past, present and future of oncolytic reovirus. *Cancers (Basel)* (2020) 12(11):3219. doi: 10.3390/cancers12113219
55. Groeneveldt C, Kinderman P, van den Wollenberg DJM, van den Oever RL, Middelburg J, Mustafa DAM, et al. Preconditioning of the tumor microenvironment with oncolytic reovirus converts Cd3-bispecific antibody treatment into effective immunotherapy. *J Immunother Cancer* (2020) 8(2):e001191. doi: 10.1136/jitc-2020-001191
56. Ghasemi F, Gameiro SF, Tessier TM, Maciver AH, Mymryk JS. High levels of class I major histocompatibility complex mrna are present in Epstein-Barr virus-associated gastric adenocarcinomas. *Cells* (2020) 9(2):499. doi: 10.3390/cells9020499
57. Parikh BA, Bern MD, Piersma SJ, Yang L, Beckman DL, Poursine-Laurent J, et al. Control of viral infection by natural killer cell inhibitory receptors. *Cell Rep* (2020) 32(4):107969. doi: 10.1016/j.celrep.2020.107969
58. Liu Z, Han C, Fu YX. Targeting innate sensing in the tumor microenvironment to improve immunotherapy. *Cell Mol Immunol* (2020) 17(1):13–26. doi: 10.1038/s41423-019-0341-y
59. Liu Z, Ravindranathan R, Kalinski P, Guo ZS, Bartlett DL. Rational combination of oncolytic vaccinia virus and pd-L1 blockade works synergistically to enhance therapeutic efficacy. *Nat Commun* (2017) 8:14754. doi: 10.1038/ncomms14754
60. Missiroli S, Perrone M, Boncompagni C, Borghi C, Campagnaro A, Marchetti F, et al. Targeting the Nlrp3 inflammasome as a new therapeutic option for overcoming cancer. *Cancers* (2021) 13(10):2297. doi: 10.3390/cancers13102297
61. Stunnenberg M, Sprokholt JK, van Hamme JL, Kaptein TM, Zijlstra-Willems EM, Gringhuis SI, et al. Synthetic abortive hiv-1 rnas induce potent antiviral immunity. *Front Immunol* (2020) 11:8. doi: 10.3389/fimmu.2020.00008
62. LaRocca CJ, Warner SG. Oncolytic viruses and checkpoint inhibitors: Combination therapy in clinical trials. *Clin Transl Med* (2018) 7(1):35. doi: 10.1186/s40169-018-0214-5
63. Motzer R, Alekseev B, Rha SY, Porta C, Eto M, Powles T, et al. Lenvatinib plus pembrolizumab or everolimus for advanced renal cell carcinoma. *N Engl J Med* (2021) 384(14):1289–300. doi: 10.1056/NEJMoa2035716
64. Makker V, Colombo N, Casado Herraes A, Santin AD, Colomba E, Miller DS, et al. Lenvatinib plus pembrolizumab for advanced endometrial cancer. *N Engl J Med* (2022) 386(5):437–48. doi: 10.1056/NEJMoa2108330
65. Finn RS, Qin S, Ikeda M, Galle PR, Ducreux M, Kim TY, et al. Atezolizumab plus bevacizumab in unresectable hepatocellular carcinoma. *N Engl J Med* (2020) 382(20):1894–905. doi: 10.1056/NEJMoa1915745
66. Tawbi HA, Schadendorf D, Lipson EJ, Ascierto PA, Matamala L, Castillo Gutierrez E, et al. Relatlimab and nivolumab versus nivolumab in untreated advanced melanoma. *N Engl J Med* (2022) 386(1):24–34. doi: 10.1056/NEJMoa2109970
67. Mahalingam D, Wilkinson GA, Eng KH, Fields P, Raber P, Moseley JL, et al. Pembrolizumab in combination with the oncolytic virus pelareorep and chemotherapy in patients with advanced pancreatic adenocarcinoma: A phase Ib study. *Clin Cancer Res* (2020) 26(1):71–81. doi: 10.1158/1078-0432.CCR-19-2078
68. Kanhere A, Hertweck A, Bhatia U, Gokmen MR, Perucha E, Jackson I, et al. T-Bet and Gata3 orchestrate Th1 and Th2 differentiation through lineage-specific targeting of distal regulatory elements. *Nat Commun* (2012) 3:1268. doi: 10.1038/ncomms2260